REGULAR ARTICLE

Growth of axile and lateral roots of maize: I development of a phenotying platform

A. Hund · S. Trachsel · P. Stamp

Abstract The objective of this study was to develop a phenotyping platform for the non-destructive, digital measurement of early root growth of axile and lateral roots and to evaluate its suitability for identifying maize (*Zea mays* L.) genotypes with contrasting root development. The system was designed to capture images of the root system within minutes and to batch process them automatically. For system establishment, roots of the inbred line Ac7729/TZSRW were grown until nine days after germination on the surface of a blotting paper in pouches. An A4 scanner was used for image acquisition followed by digital image analysis. Image processing was optimized to enhance the separation between the roots and the background and to remove image noise. Based on the root length in diameter-class distribution (RLDD), small-diameter lateral roots and large-diameter axile roots were separated. Root systems were scanned daily to model the growth dynamics of these root types. While the axile roots exhibited an almost linear growth, total lateral root length increased exponentially. Given the determined exponential growth, it was demonstrated that two plants, germinated one day apart but with the same growth rates differed in root length by 100%. From the growth rates we were able to identify contrasting genotypes from 236 recombinant inbred lines (RILs) of the CML444 x SC-Malawi cross. Differences in the growth of lateral roots of two selected RILs were due to differences in the final length and linear density of the primary lateral roots, as proven by the manual reanalysis of the digital images. The high throughput makes the phenotyping platform attractive for routine genetic studies and other screening purposes.

Keywords Digital image analysis · Corn · Early vigor · Root growth · Root morphology · Seedling vigor · Zea mays L

Abbreviations

CMYK	cyan, magenta, yellow and key (black)
DAG	days after germination
ER_{Ax}	elongation rate of axile roots
HSV	hue, saturation, value
k_{Lat}	relative elongation rate of lateral roots
QTLs	quantitative trait loci
RGB	red, green, blue
RIL	recombinant inbred line
RLDD	ziameter-class distribution

A. Hund (✉) · S. Trachsel · P. Stamp
Institute of Plant Science, ETH Zurich,
8092 Zurich, Switzerland
e-mail: andreas.hund@ipw.agrl.ethz.ch

Introduction

In the past, considerable efforts were made to develop a suitable method for the study of roots leading to a number of different methods. These methods differ

mainly in the resolution in time and space as well as in throughput. Insight into root systems of different species was obtained already at the beginning of the 20th century by excavating whole root systems (Weaver 1925). Other approaches focus either on roots growing in large root chambers and monitored at the surface of acrylic glass in soil-filled root observation chambers (Manschadi et al. 2006; Manschadi et al. 2008), on X-ray imaging (Doussan et al. 2006; Gregory et al. 2003), or on destructive sampling from soil columns (Hund et al. 2008b). Despite the advantage that the root growth of crops can be evaluated until maturity, the throughput of these systems is usually not high enough for the assessment of large sets of genotypes as needed for mapping studies of quantitative trait loci (QTLs). At the other extreme, some systems focus on the early growth of the primary axile root a few days after germination. These high-throughput systems are usually designed to assess the stress response of the root system and to allow for a high resolution in time, e.g. by time laps analysis of the growth of the root apical meristem (Walter et al. 2002). While root measurements at the later developmental stages of a crop lack throughput, systems that measure the growing tip of the primary axile root neglect the development of lateral roots which, are an important part of root system. Roumet et al (2008) pointed out that whole root system traits did not allow strong predictions of root respiration and exudation among three major plant families (Asteraceae, Fabaceae and Poaceae). The authors attributed the lack of prediction to the fact that these processes are more linked to fine roots than to whole root system traits. There are numerous examples of differences in the development of lateral roots among genotypes. Lateral roots play an important role in the plant's ability to access water (Varney and Canny 1993) and nutrients such as phosphorus (Lambers et al. 2006). In maize, they may also be important for vigorous growth at low temperature (Hund et al. 2008a; Hund et al. 2007). By contrast, genetic variation in the growth rates of axile roots in maize may be exploited for a better acquisition of water from deep soil layers (Hund et al. 2008b) or a better N efficiency (Liu et al. 2008).

We designed a system for the rapid measurement of the root system during the first days of lateral root growth in growth pouches. Growth pouches are inexpensive and space-saving, facilitating the two-dimensional observation of root growth over time on the surface of a blotting paper. The system enables the investigation of root elongation of maize for about the first 10 days after germination (DAG). To date, growth pouches have been used for different plant species and different purposes. Janssen et al. (1995) screened potato for resistance to root-knot nematodes, McMichael and Burke (1998) studied the effect of temperature on the root growth of cotton, Bonser et al. (1996) examined the effect of phosphorous availability on the orientation of basal roots of *Phaseolus vulgaris,* while Liao et al. (2004) mapped QTLs for the same trait. Liao et al. (2001) observed that gravitropic responses to phosphorous availability after six days in growth pouches was consistent with growth patterns after 4 weeks in solid media. They also observed that the morphology of basal roots of bean showed a high correlation between plants grown in pouches and in soil. The root parameters measured in growth pouches were highly correlated with those measured in pots of sand and soil (Bonser et al. 1996) and were consistent with several traits found in field trials (Liao et al. 2001; Liao et al. 2004). This supports the utility of growth pouches for screening of genotypes. So far the system has not been optimized to study the growth dynamics of roots in combination with digital image analysis. The specific aims were i) to develop a simple, high throughput system to assess the growth dynamics of axile and lateral roots of maize using digital imaging, ii) develop a protocol for an automated analysis of these images and iii) test the ability to identify genotypes with contrasting root morphology.

Material and methods

The maize inbred line Ac7729/TZSRW (P2) was used throughout the system establishment. For the manual measurement of different root types in the image processing software Photoshop (Photoshop 7.0, Adobe Systems Inc., San Jose, CA, USA), two contrasting recombinant inbred lines (RILs) were chosen. This choice was based on an unpublished evaluation of root growth of a set of 236 RILs of the CML444 x SC-Malawi cross (Messmer 2006) supplied by CIMMYT. RIL 372 had a lower elongation rate of the lateral roots compared to RIL 15.

Genetic material and growth conditions

Germinated seeds were transferred to moistened blotting paper of 21×29.5 cm (Anchor Paper, St. Paul, MN, USA) in pouches. The pouches consisted of a 0.5 mm strong opaque polyethylene foil 22× 60 cm (PE-Teichfolie Typ WA-1200, Walser Kunststoffwerk AG, Buerglen, Switzerland) folded to obtain a pouch of 22×30 cm with the short edge closed (Fig. 1a). Half way along the short edge (upper side of the pouch), a hole (5 mm in diameter) was cut to allow the emergence of the coleoptile; 3 cm below that hole, a bulge (10 mm diameter, 5 mm depth) was

molded on the front side of the pouch to keep the seed in place. The seed was fixed with two standard paper clips, one on each side of the bulge. The pouch was attached to a rod with two foldback clips (Jakob Maul GmbH, Bad König, Germany), one on each side of the upper edge of the pouch.

The pouches were hung into plastic containers (27×37×32 cm ; Arcawa GmbH, Chatillon, Switzerland) so that the lowest 2 cm of the blotting paper were submerged in 4 l nutrient solution (Fig. 1b). The nutrient solution consisted of 0.23% Wuxal (Aglukon Spezialdünger GmbH, Düsseldorf, Germany (16 mM N; 1 mM P_2O_5; 2 mM K_2O; 7.8 mM Fe; 6.7 μM Mn;

Fig. 1 Growth pouches consisted of blue germination blotter covered with a black PE foil, 0.5 mm thick (a). The different components were held together by paper clips. Growth pouches were placed in plastic containers (b). Roots were scanned with a conventional scanner (d) with a resolution allowing for the separation of axile (Ax) and lateral (Lat) roots (c) (Genotype: RIL 15 at 9 DAG)
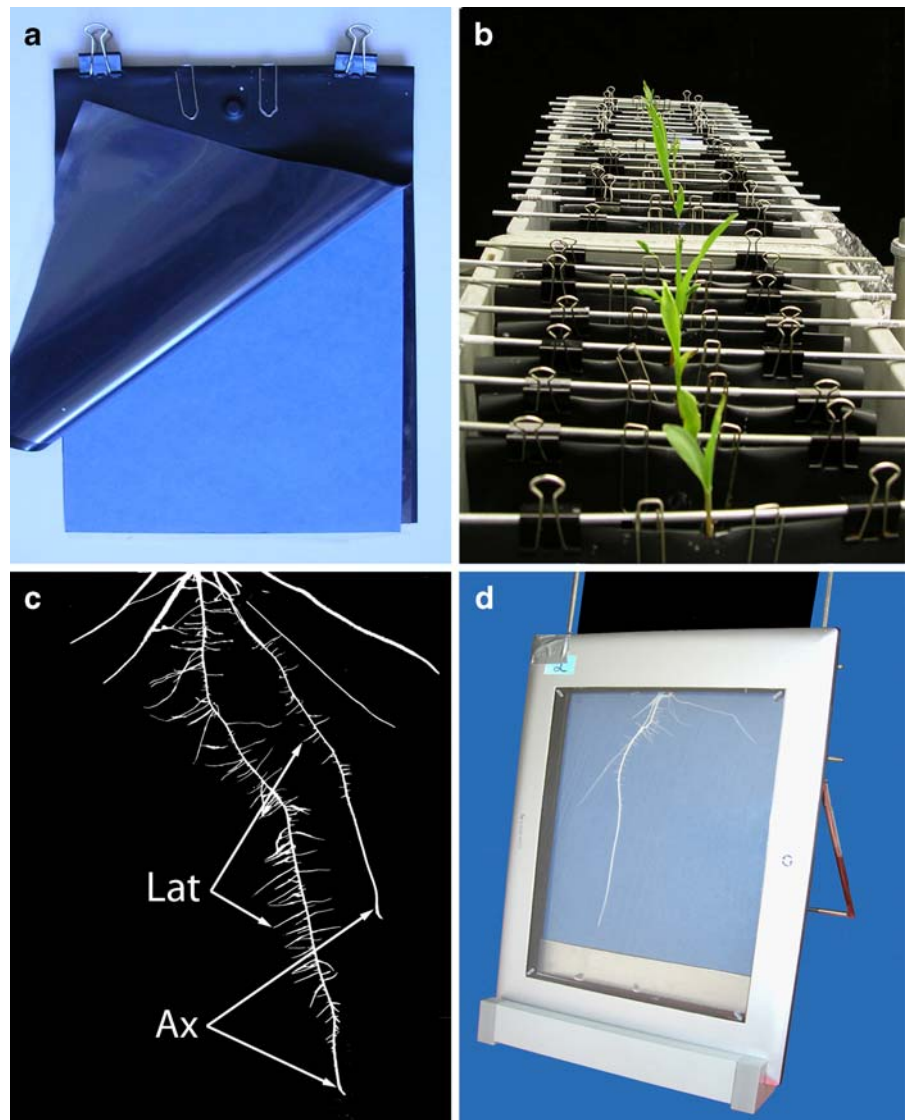
21.3 μM B; 2.9 μM Cu; 2.2 μM Zn and 1.1 μM Mo)). The containers were placed in a growth chamber (PGW36 Conviron, Winnipeg, MB, Canada) at a temperature of 27°C at the seed level, a relative humidity of 70%, a photosynthetic active radiation of 400 μmol sec^{-1} m^{-2} and a photoperiod of 12 h. To avoid heating of the pouches, the containers were covered with aluminum foil, leaving an opening 2 cm wide through which the seed grew.

Acquisition and processing of images

A Hewlett Packard Scanjet 4670 "See Thru Vertical Scanner" (Hewlett-Packard, Palo Alto, CA, USA) was used for image acquisition. The Scanjet was placed vertically on its short edge (Fig. 1d). The surface of the blotting paper was 5 mm from the scanner surface to avoid direct contact with the roots. Images were obtained with a custom software using the TWAIN interface. The software stores a time-stamp in the image names used as covariates in the linear models (t$_j$s in Eq. 1). Images were scanned as 24 bit RGB (red, green, blue) color with a resolution of 23.7 dots mm^{-1} (600 dpi) and a scanning area of 19×24 cm. Files were stored as JPEG (Joint Photographic Experts Group) with the highest quality.

Images were pre processed in Photoshop followed by digital images analysis in WinRHIZO (Version 2003b, Regent instruments, Montreal, QC, Canada) as outlined in Fig. 2. Photoshop was used to i) decompose the 24 bit images into their 8 bit color cannels, ii) remove image noise from these channels by applying a median filter and iii) apply an appropriate threshold tonal value to the respective channel to separate into roots and background. Details about the optimization process are given in the next section. Out of 11 tested color channels, the saturation channel was the choice to generate 8 bit images for routine analyses. These 8 bit images were smoothed, using the median filter (Filter > Noise > Median) with a radius of three pixels before setting an appropriate threshold to generate binary images containing the information allowing for a better distinction of objects (roots) and background (Fig. 1c).

WinRHIZO was used to detect the root length in the image. The diameter classes were set at the size of 42 μm, the equivalent of one pixel. The debris removal filter of WinRHIZO was set to remove objects with an area smaller than 0.02 cm^2 and a
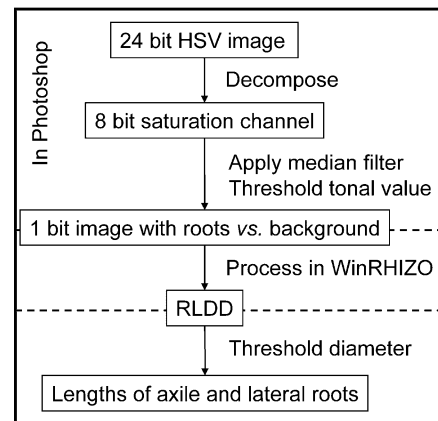
Fig. 2 Image processing steps after optimization

length/width ratio lower than 5. The software's output of the root length in diameter-class distribution (RLDD) was used to separate into axile and lateral roots. In order to detect the position of the trough, none parametric local polynomial fits of second order and a neighborhood proportion of 40% (span, $\alpha=0.4$) were fitted to the RLDD using the R function loess() (R Development Core Team 2008).

Evaluation of test images for system establishment

A set of 18 plants of P2 was grown in pouches and scanned daily between 3 and 8 DAG. Out of these, pouches with well developed plants were chosen for further processing. The establishment of image processing steps as outlined in Fig. 2 is described in the following.

Decomposition of 24 bit images to 8 bit

To choose a color channel for thresholding, separating best between roots and background, the roots scans of 8 DAG were separated manually from the blue background of the blotting paper by means of the magic wand tool in Photoshop. These color images were decomposed in their underlying 8-bit color channels using Photoshop and its plugin Curvemeister 2 (Curvemeister, Berkeley, CA, USA). The plugin was used, to decompose the images into the HSV color space. If necessary, channels were inverted so that all images displayed white roots on dark background. The channels used to decompose the images were i) an average of the three basic RGB

color channels according to the formula Y=0.3R+ 0.59G +0.11B (the default grayscale conversion), ii) the channels of the RGB color space, iii) the channels of the CMYK color space (cyan, magenta, yellow and key (black), and iv) the channels of the HSV color space (hue, saturation, value). The frequency distribution of the 256 levels (tonal range) of each 8-bit channel was extracted by the Photoshop plugin Hisotext (Thain 2005). According to the Histotext output (*cf.* Fig. 3), the threshold tonal value for obtaining binary images was set in a way that, on average, 0.1, 0.5, 1, or 5% of the pixels in the background images were falsely classified as objects. The respective threshold was then applied to the object images to obtain the proportion of object pixels falsely defined as background (Table 1).

Separation into axile and lateral roots after processing of binary images with WinRHIZO

After processing the images in WinRHIZO, the RLDD of 12 series of images was used to establish separation into axile and lateral roots. First, the dynamic of the RLDD values over time was used to evaluate the evolution of the putative peaks of the lateral and axile roots. Second, two time points of these series of images were used for verification: i) the time point where the putative peak of the lateral roots had just emerged and ii) the images of the last scan (*cf.* Fig. 6). In the corresponding binary images, axile and lateral roots were separated manually using Photoshop. The separated images, representing either axile or lateral roots, were then processed in the same way as the original images.

Data processing and statistics

Successive scans were modeled as repeated measurements within plots. Each plot consisted of one pouch containing one plant. To determine whether, axile and lateral roots grew exponentially or linearly, the samples were analyzed with the R function nlme() from the nlme package (Pinheiro et al. 2004). The following mixed non-linear model was fitted:

$$y_{ij} = (\beta_1 + b_{1i})t_j + (\beta_2 + b_{2i})e^{(\beta_3 + b_{3i})t_j} + \varepsilon_{ij} \qquad (1)$$

where y_{ij} is the root length of plant i at DAG j, βs are the mean values of the parameters of the population of individual plants, bs are the deviations of the individual plots. β_1 and b_{1i} are the linear elongation rates, β_2 and b_{2i} are the intercepts, β_3 and b_{3i} are the rate constants and t_j is the time at which the individual plots were measured in DAG. The time to calculate DAG was derived from the timestamp added to the image name by the scanning software. Based on the
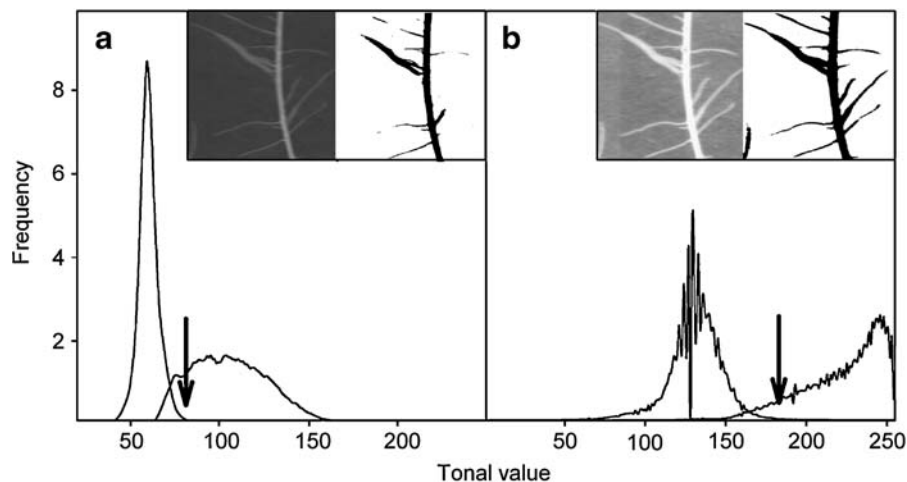
Fig. 3 Frequency distribution of tonal values of the background (left peak) and target objects, i.e. roots (right peak) for the classical gray scale mode (a) and for the saturation channel (b). Gray scale inserts show a representative detail of the original images in gray mode (a) or as saturation channel (b).

Black and white inserts show the results after applying a threshold tonal value of 83 (a) or 183 (b) (arrows). The thresholds were selected to result in the same 0.5% noise in the background images (*cf.* Table 1)

significance of the terms in the model, elongation of the axile roots was modeled using the full model, while the elongation rate of the lateral roots was modeled using the exponential term only (*cf.* Fig. 7). In the latter case, $\beta_3 + b_{3i}$ denotes the relative elongation rate of lateral roots (k_{Lat}) of each individual plant.

Manual examination of images

Five series of images of RIL 15 and RIL 372, scanned at 3, 5, 7 and 9 DAG, were examined by means of the measure tool of Photoshop. In each image, the following traits were assessed on the primary root and on the first seminal root: length of the axile root, length of the first three lateral roots, which emerged from that axile root (proximal lateral roots), length of the longest lateral root at 9 DAG, number of lateral roots and their linear density (number of lateral roots divided by the length of the branched zone). Furthermore, the lag phase until the first lateral roots appeared was determined as the time between germination and the last day, on which the image did not display any lateral roots. Finally, the number of axile roots was determined. Since the shoot base was not visible in the images, we were unable to distinguish between seminal axile and crown axile roots.

Table 1 Misclassified object pixel (%), depended on the threshold applied to the tonal values of each channel of the three major color spaces of a 24 bit color image (RGB, CMYK, HSV)

Color channel	Misclassified background pixel (%)			
	5	1	0.5	0.1
	Misclassified object pixel (%)			
Saturation	1.5	5.7	9.6	29.5
Cyan	1.4	6.3	11.0	30.9
Red	1.2	7.4	13.1	30.4
Magenta	2.5	9.1	14.9	34.1
Gray mode	3.1	11.6	16.4	32.9
Avsed[a]	2.27	3.00	3.29	3.66

The threshold was determined for each color channel based on background images allowing for 5, 1, 0.5, or 0.1 % of background pixel being classified as object. Only color channels with improved classification compared to the gray scale mode are displayed

[a] Average standard error of the difference

Mixed linear models were fitted based on either the values obtained from the analysis of the last image or the temporal dynamics of these values over the four scanning dates. The models were fitted using the R function lme() of the nlme package (Pinheiro et al. 2004). For the temporal development the complete quadratic model with respect to the time (DAG) covariant was:

$$y_{ijkl} = g_i + a_j + t_k + t_k^2 + gt_{ik} + at_{jk} + gt_{ik}^2$$
$$+ at_{jk}^2 + gat_{ijk} + gat_{ijk}^2 | r_l + g_{li} + a_{lij}$$
$$+ \varepsilon_{ijkl} \tag{2}$$

where y_{ijkl} is the trait value of root type a_j (primary or seminal axile roots) within genotype g_i (RIL 15 or RIL 372) within replication r_l (l=1,…,6) at time t_k (k=1,…, n_{lij}). Due to different lag times until the roots emerged, the number of temporal observations n_{lij} on each root type per plot and replication differed. Only two observations were available for some of the plots, while for others four observations were available. Random effects are those to the right of the vertical line in Eq. 2. The final formulation of the model resulted from backward selection based on the p-value with a probability threshold at 0.05.

Results

The saturation channel granted the best contrast between roots and background

Appropriate image processing is a crucial step for the distinction between object and the background in a digital image. For this purpose we manually separated the background and the objects in nine images. The percentage of falseley classified pixels in the object images was estimated given a certain percentage of noise in the background image. This was done for each channel of the three used color spaces as well as for the standard gray mode. For example, allowing 0.5% noise in the background image, the saturation channel of the HSV color space yielded a tonal value of 183 (Fig. 3b; arrow) as the threshold for the separation of the object from the background. Applying this threshold to the object images resulted in a false classification of an average of 9.6% of all pixel as background. By contrast, using the same background

noise for the gray mode, i.e. a tonal value of 83 (Fig. 3a; arrow), yielded a significantly larger percentage of falsely assigned object pixels (16.4%). The effects of these differences in object detection are visualized in the inserts of Fig. 3. Given a noise in the background images of 0.1, 0.5, 1 and 5%, the saturation channel generally showed the lowest proportion of falsely classified pixels in the object images (Table 1). Inserts in Fig. 3a visualize the loss of roots in the binary image derived from the gray-mode. By contrast, the inserts in Fig. 3b visualize the detection of roots in the binary images derived from the saturation-channel.

The root length in diameter-class distribution was suitable for discrimination between axile and lateral roots

The RLDD recorded between 3 and 8 DAG shows the development of a multimodal distribution over time (Fig. 4), where two distinct peaks were expected, one for the axile roots and one for the lateral roots. Observing the development of the peaks over time, suggested that the peak below 0.5 mm, developing after 6 DAG, belonged to the lateral roots. A representative series of images (Fig. 5) illustrates the emergence of the first two short lateral roots at 5 DAG, with the lateral roots increasing in number over the following days. Above 0.5 mm, smaller peaks in the RLDD formed at about 0.65, 0.95 and 1.2 mm (dotted lines in Fig. 4). These may be the result of either roots that were growing in parallel to each other, artifacts generated by the software, or roots with distinct diameter classes. Since we were not interested in resolving differences in root diameters within the axile and lateral roots, the neighborhood proportion of the LOESS smoothing function was set to resolve a bimodal distribution. The trough between the two peaks was clearly detectable at 7 and 8 DAG. However, it changed from 0.48 mm at 7 DAG to 0.68 mm at 9 DAG (Vertical lines in Fig. 4). In order to elucidate, if this increase was a result of an increasing overlapping of the lateral roots, either lateral or axile roots were removed from the images in Photoshop and processed separately in WinRHIZO (Fig. 6). The RLDD showed a clear distinction for peaks generated from images containing either axile or lateral roots. This was the case at 6 DAG, when lateral roots were just beginning to emerge, and at 8 DAG when a considerable number of lateral roots had already formed. The major portion of the root lengths belonging to the small peak at about 0.65 mm was formed by axile roots.
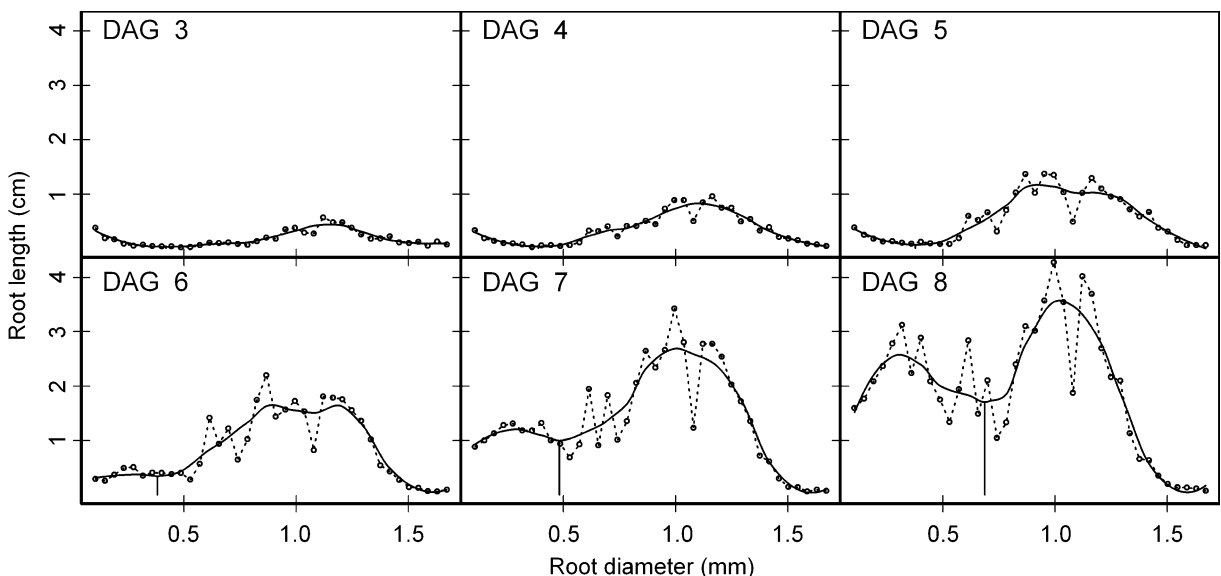
Fig. 4 Root length in diameter-class distribution generated by the WinRHIZO (dotted lines) and after LOESS smoothing (solid lines) on different days after germination (DAG). Each dot represents an average o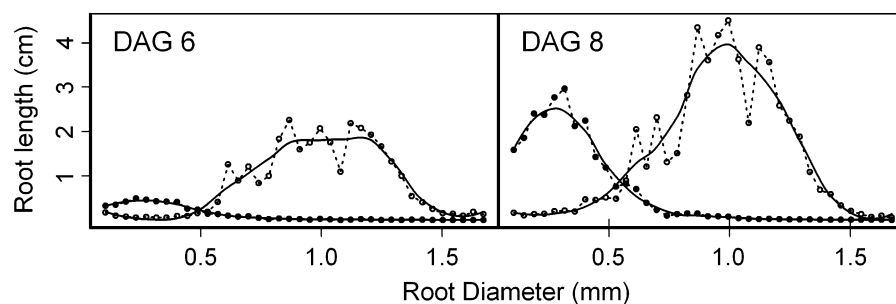f 12 observations at the mid point of the respective diameter class. Vertical lines indicate the trough between the peak putatively representing the lateral roots and the peak putatively representing the axile roots

Fig. 5 Sequence of image of the root development of inbred line P2 in a growth pouch. Numbers indicate the day after germination. The plant developed one primary root (long and branched) and one seminal root (unbranched). The seed was not scanned

Axile roots tended to elongate linearly, whereas lateral roots grew exponentially

Roots in the images were measured until the first axile roots grew out of the pouch, which occurred usually between 8 and 9 DAG. When axile roots had grown out of the pouch, they were placed back on the

blotting paper surface during scanning. A first observation of the development of the axile and lateral roots over time suggested a more linear elongation of the axile roots and exponential elongation of the lateral roots (Fig. 7). The final models, derived from Eq. 1, confirmed the exponential growth of the lateral roots since only the exponential term in the model was significant. The relative elongation rate of the lateral roots was 0.763 cm d^{-1}, reflecting a doubling of root length every 0.91 days.

A linear-exponential model was suggested for the axile roots, because both the linear and the exponential term were significant. The elongation rate of the axile roots (ER_{Ax}) was 2.93 cm d^{-1} (Fig. 7); the relative elongation rate was 0.51 cm d^{-1}. The exponential component may reflect the increase in axile root numbers over time.

Differences in germination lead to a considerable overestimation of the exponentially elongating lateral roots

In large populations of about 200 individuals, there may be considerable differences in germination due to i) random environmental effects and ii) genetic differences among genotypes. Based on the growth parameters derived from Eq. 1 we estimated potential errors due to such differences (Fig. 8a and b). Figure 8a and b demonstrate that a faster germination by one day at the same growth rate, leads to a very large, constant overestimation by 115% of the exponentially growing lateral roots (Fig. 8b). Germination effects on the axile root lengths were different. Following a linear-exponential growth function, their length was strongly overestimated at the beginning of the experiment and

Fig. 6 Root length in diameter-class distribution of axile roots (open circles) and lateral roots (closed circles) at 6 and 8 days after germination. Roots in the original images, used to generate

Fig. 6, were separated and images containing either axile or lateral roots were generated. For further details see Fig. 4
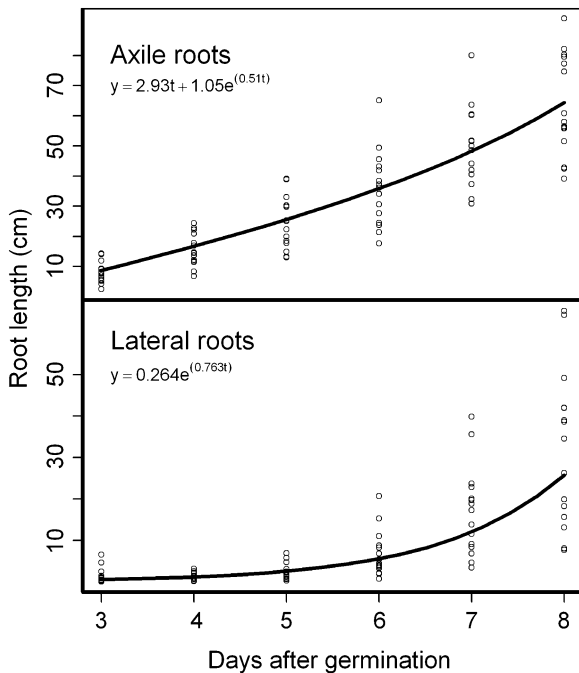
Fig. 7 Growth curves of the axile and lateral roots. Circles indicate root lengths detected in individual images. Lines represent the fitted regressions based on model 1

the length of the lateral roots was log-transformed, the overestimation at 10 DAG due to differences in germination was reduced to 19% for the lateral root length and −9% for the ratio between the lateral and axile root lengths.

Elongation rates determined in the growth pouches can be used to identify genotypes with different root morphology

We used the CML444 x SC-Malawi QTL population to elucidate the cause of differences in the relative elongation rates of lateral roots of two of the most different RILs for this trait. RIL 15 had a higher k_{Lat} compared to RIL 372 (Table 2) thus contributing to the four fold increase of lateral root length at 9 DAG (Table 2, Fig. 9). On the other hand, the ER_{Ax} of RIL 15 was only half that of RIL 372. Note that the elongation of axile roots over time of this population followed a linear function (data not shown).

The measurements of the original images, carried out using the measure tool of Photoshop, revealed the dynamics of the components of the root systems. Plots of the mean values of the components of the primary and seminal root of the two genotypes suggested linear elongation of the axile roots (Fig. 10 a) and an exponential increase in the number of lateral roots over time (Fig. 10e). For the other root parameters, the growth dynamics depended on the genotype and root
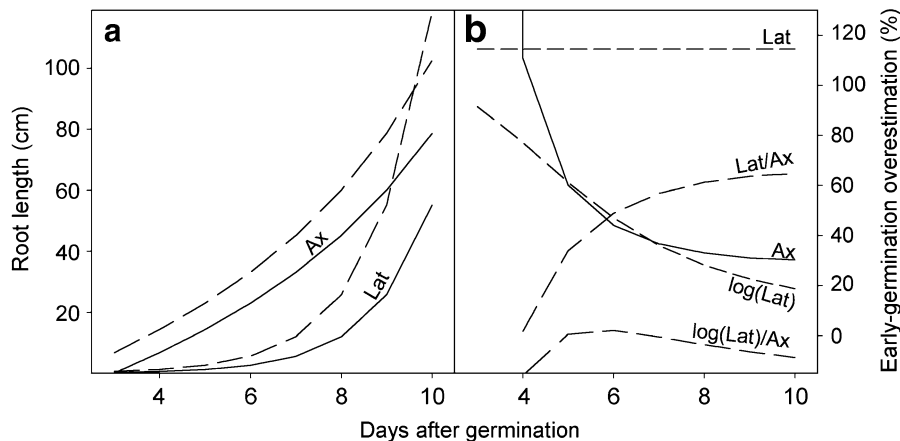
the values decreased asymptotically over time to about 30% at 10 DAG (Fig. 8b). Consequently, the overestimation of the ratio between the lateral and axile root lengths increased asymptotically from 2 to 65%. When

Fig. 8 Errors due to differences in growing time. Hypothetical plants with the same elongation rates of axile roots (Ax) and lateral roots (Lat). Growth functions were derived from Fig. 7. Plant one (a; dashed lines) germinated one day earlier than plant two (a; solid lines). The length advantage due earlier germination b) depends on the growth function of the root types. When lateral root length was log transformed and these data were also used to calculate the ratio between the lateral and axile root lengths (log(Lat)/Ax), the overestimation due to earlier germination decreased with time

Table 2 Results of ANOVA and mean values of root traits of two contrasting recombinant inbred lines (RILs) of the CML444 x SC-Malawi cross: Growth constant of lateral roots (k_{Lat}), the end length of the lateral roots (L_{Lat}), elongation rate of axile roots (ER_{Ax}), the k_{Lat}/ER_{Ax} ratio and the number of axile roots (#Ax) at 5 and 9 days after germination (DAG)

|	k_{Lat} cm d^{-1}	L_{Lat} cm	ER_{Ax} cm d^{-1}	k_{Lat}/ER_{Ax}	#Ax DAG 5 Numbers	#Ax DAG 9 Numbers
ANOVA	***	***	***	***	***	ns
RIL 15	0.533	113	7.5	0.0714	1.60	3.80
RIL 372	0.416	27	14.1	0.0307	4.25	5.00

The RILs were chosen based on differences in k_{Lat} calculated from the WinRHIZO output

type. The plots of the temporal increase in the proximal lateral roots (Fig. 10b) and the longest lateral root (Fig. 10c), suggested an asymptotic increase for RIL 372 and a linear increase for RIL 15. This, in turn, suggests that the lateral roots of RIL372 reached their final length during the course of the experiment, while those of RIL 15 were still elongating. The number of axile roots increased rapidly between DAG 3 and 5 for RIL 15 and than stagnated, while the number of axile roots increased at slower but constant rates for RIL 372 (Fig. 10d). The linear densities of all roots increased during the first two days after their appearance and remained more or less constant afterwards (Fig. 10f). The lag time, during which no lateral roots were visible, varied from 3 to 5 DAG (Table 3). The seminal lateral roots developed about one day earlier than those of the primary root.

Based on observations from Fig. 10, the temporal changes in the length of the axile roots and the number of lateral roots were modeled using all time points, while the differences at 9 DAG were examined for the remaining traits (Table 3). For the length of the axile roots, all quadratic terms (*cf.* Model 2) and the intercept and slopes of the genotypes were not significant. The axile roots of RIL 15 were initially longer and grew faster compared to the seminal root, while the axile and seminal roots of RIL 372 had equal intercepts and slopes. For the number of lateral roots, the intercepts (root number at root appearance) were not significant. Therefore, only the slopes are presented in Table 3. The quadratic term was significant for the overall increase of lateral roots ($1.2*t^2$; data not shown) but not for the interactions. This indicates that the number of lateral roots of genotypes and root types deviated linearly from the overall increase. The linear increase of the number of primary lateral roots of RIL 15, with 21 roots per day, was comparably strong, whereas the increase in the

Fig. 9 Representative images of two recombinant inbred lines of the CML444 x SC-Malawi cross at 9 DAG. The RILs were selected based on their differences in k_{Lat}. Vertical stripes are artifacts of the scanner when operated with a 5-mm distance from the blotter. Longest roots grew out of the pouch and were placed on the blotter paper for scanning
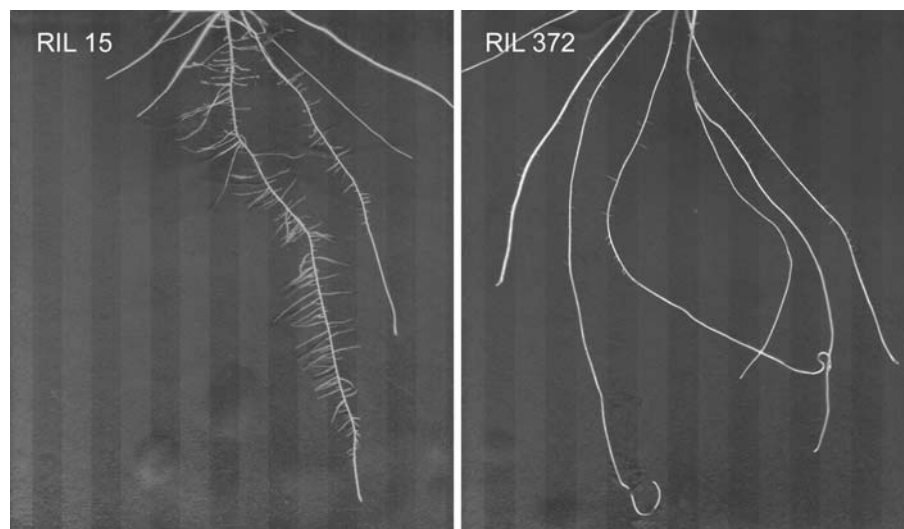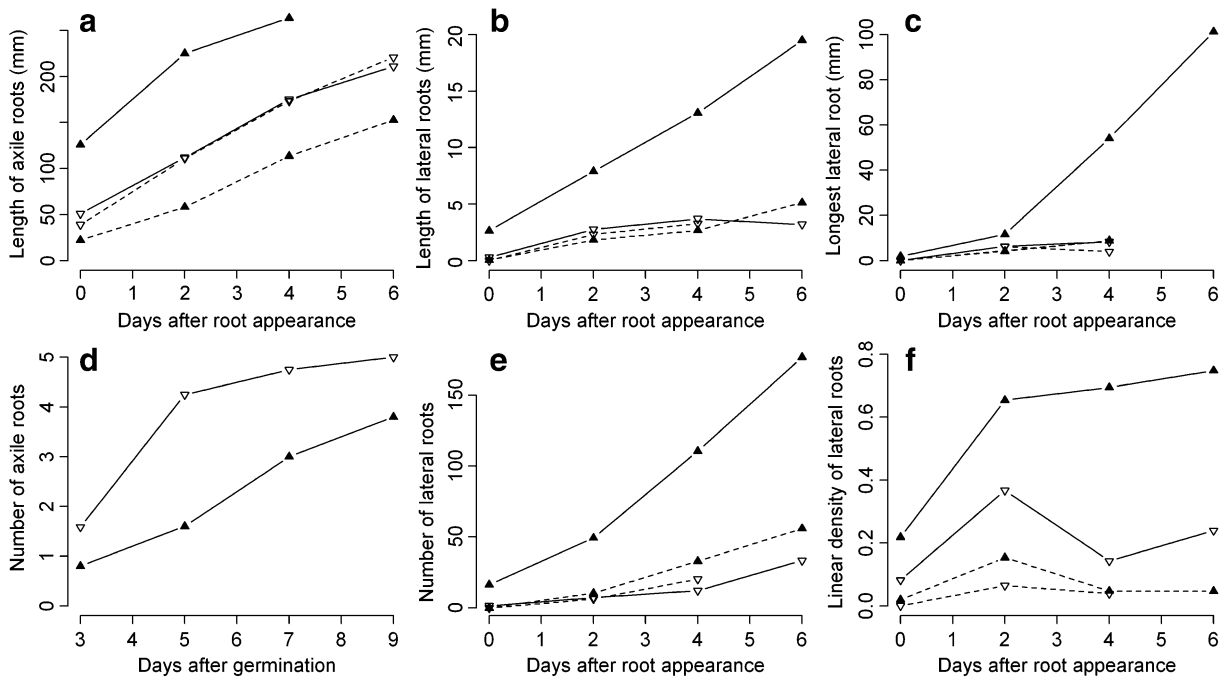
Fig. 10 Manual measurements of characteristics of the primary root (solid lines) and the first developing seminal root (dashed lines) of RIL 15 (closed triangles) and RIL 372 (open triangles) as dependent on time: lengths of the axile roots (a) the proximal lateral roots (b) and the longest lateral root (c); numbers of axile (d) and lateral roots (e); linear density (# mm^{-1}) of lateral roots in the branched zone (f). Five image series were evaluated per genotype

number of lateral roots of the other root types was much lower, in the range of ±2 roots per day. Note that slopes are negative since the estimates for t^2 were not included in the linear combination. In summary, the root system of RIL 15 was characterized by a strong primary root in comparison to the other roots. This primary root showed at least a four-fold increase of the following traits: number of laterals, length of proximal and longest lateral roots and linear density of lateral roots at 9 DAG. However, the values of the seminal roots for RIL 15 did not differ greatly from those of RIL 372.

Discussion

Image processing

WinRHIZO usually processes 8-bit images (256 levels of gray) by applying an automatic or user-defined gray-scale threshold to generate binary images distinguishing between the roots (objects) and the background. Alternatively, these binary images can be generated in external software such as Adobe Photoshop 7.0. Pre processing the images allows making use of additional options to differentiate between roots and background, image smoothing and manual control of the binary images prior to the processing in WinRHIZO.

We enhanced the discrimination between object and background by using the saturation channel instead of converting color images to the standard gray mode. Making use of the different color spaces is one option to improve the discrimination between roots and background. Another option considered, was to use color statistics to identify those colors, among the more than 16 million possible ones, belonging to roots or background, only. Since this color analysis was not available in standard software, such as Photoshop, the use of the color spaces was chosen as the best and most flexible solution.

We smoothed images using the Median filter in Photoshop. WinRHIZO offers a similar "image smoothing filter" recommended when analyzing "large, hairy roots"; the filter applies an undefined blurring function to the image to avoid "noisy"

Table 3 Results of ANOVA and main effect of genotype (RIL 15 or RIL 372) and root type (primary or seminal root), on final length of roots proximal to the shoot base (prox.) and the longest lateral root (long.); final linear density of lateral roots per mm axile root; growth period without visible lateral roots (lag time); intercepts (int.) and slopes (slp.) of the temporal dependence of axile roots (L_{Ax}); slope of the temporal dependence of the number of lateral roots ($\#_{Lat}$)

		Final root length		Linear density	Lag time	L_{Ax}		$\#_{Lat}$
		prox. mm	long. mm	$\# \ mm^{-1}$	d	int. mm	slp. $mm \ d^{-1}$	slp. $\# \ d^{-1}$
Int./slp.		***	***	***	***	***	***	***
Genotype (G)		**	***	***	ns	-[a]	-	***
Root type (R)		***	***	***	***	***	*	***
G:R		***	***	***	ns	***	*	***
Root type	RIL							
primary	15	15.44	86.75	0.744	3.03	126.78	37.48	21.25
primary	372	3.66	6.41	0.165	3.90	59.05	29.24	−2.42
seminal	15	1.79	5.38	0.027	5.43	18.63	18.85	1.55
seminal	372	3.24	6.70	0.046	4.90	54.95	32.83	−1.22

The slopes are given by the respective treatment-by-time interactions

[a] Terms that were dropped from the model are indicated by "-"

skeletons. This filter is suitable for the 8-bit source images but of minor use for binary images and was therefore turned off.

We calculated the lengths of the axile and lateral roots, respectively, using the root lengths above and below a certain threshold in the RLDD. A scanner was used to acquire high resolution images with about 28 megapixel (24 px mm^{-1}). A large image resolution is crucial for the unambiguous separation of roots of different diameter classes and not yet achieved by standard digital cameras in the desired dimensions. Richner et al. (2000) and Zobel (2003) proposed a pixel size that is one third and one quarter of the smallest root diameter, respectively. The first-order lateral roots of maize are in the range of 100 to 800 μm (Varney et al. 1991). The authors distinguished four classes of lateral roots of maize with the majority of roots in the two lowest classes (average diameter ranging from 214 to 350 μm). The used image resolution of 23.7 dots mm^{-1} is five times smaller than the smallest root class reported by Varney et al. (1991). Therefore, the chosen resolution is well suited to detect all maize roots in the image and distinguish between axile and lateral roots. However, the resolution is not high enough to explore the nature of the additional peaks detected for the axile root or to resolve different diameter classes

within the population of lateral roots. In order to achieve this, a resolution of 94 p mm^{-1} in combination with an appropriate smoothing function would be needed (Zobel 2008). One reason for the need of such a high resolution, are artifacts generated by WinRHIZO (Zobel et al. 2007). These artifacts may be responsible for the dips and peaks observed at regular intervals in the RLDD (Fig. 4). These dips and peaks were at the same place at every developmental stage and were also detected in the individual images (data not shown). Zobel (2008) examined the nature of the artifacts and summarized that the observed dips occur every 3 to 4 pixel (occasionally two and five) widths along the x-axis (diameter-class distribution). It was suggested that the observed dips occur due to the lack of uniformity in the pattern of width decrease with increasing angle among width classes.

Effects of delayed germination of measured root traits

We demonstrated that a delay of one day in germination can lead to an overestimation of the length of the lateral roots by over 100%. Most genetic analyses of the development of the root system included an assessment of the plants at a very early stage of growth. Under near-optimal conditions, maize seedlings grew until not more than 12 DAG

(Hoecker et al. 2006; Hund et al. 2008a; Zhu et al. 2005) to 21 DAG (Tuberosa et al. 2002), reflecting a harvest at about the V1 to V2 growth stage. Differences in germination are common in large populations and may lead to the errors described above when not taken into account. For example, Hund et al. (2004) observed differences of almost three days in the germination of RILs of a QTL mapping population. Two QTLs, which increase the length of the primary lateral roots, co-located with a small germination index (fast germination). These loci are probably germination loci rather than root morphological loci. Another example is the study of initiation of lateral roots and hybrid vigor (Hoecker et al. 2006). The axile root length was measured daily from 3 to 7 DAG. The root length of some of the hybrids was significantly higher than that of the mid-parent value throughout the experiment, but there was no visible difference in the slope. This indicates differences in germination rather than growth of the axile root. Therefore, it is recommended, to check the dynamics of the root type, so that the appropriate measures can be taken. At the early stage, when root systems are measured at a certain point in time and differences in germination are not considered, it is suggested that the length of the lateral roots is log-transformed in order to reduce errors.

Influence of seed reserves on root morphology

Root morphology at the early growth stage is strongly influenced by the carbohydrate supply by the seed (Enns et al. 2006). The authors showed that the removal of the endosperm decreased the density and the length of the rootbranches in the basal 10 cm region of the primary root. This indicates that seed quality and the availability of endosperm reserves may be important triggers of root morphology. Autotrophic growth of maize seedlings lasts until about 9 to 10 DAG (Bourdu and Grégory 1983; Cooper and Mac Donald 1970; Delées et al. 1984), the timeframe of many genetic studies. The extent, to which seed quality has pleiotropic effects on root morphology has yet to be determined. However, differences in early root morphology are important, independent of their cause. The root system is important for phosphate uptake before the V2 stage, highlighting the importance of an early increase in the length and density of lateral roots (Chassot and

Richner 2002). Furthermore, Hund et al. 2007, 2008a outlined the correlation of the length and density of lateral roots with early growth and photosynthetic performance under chilling stress conditions.

Dissection of causes for different elongation rates of roots based on their underlying morphological components

Based on the manual observations of the two contrasting RILs in Photoshop, it is concluded that the differences in k_{Lat} were due mainly to a difference in the morphology of the primary root of RIL 15. This RIL had an increased elongation rate of the primary axis with a greater linear density of lateral roots and a greater and constant elongation rate of these roots during the course of the experiment. This is in line with theoretical considerations: The population of lateral roots of a single root elongates exponentially during the initial phase of its development. This exponential increase is caused by a steadily increasing number of growing roots tips. The exponential growth continues until the final length and density of the oldest proximal lateral roots are reached. Thereafter, the population of lateral roots is expected to elongate linearly. This may seem to be an oversimplification, because laterals may sometimes be extremely long and initiate higher-order laterals (McCully 1999). However, we did not observe this for the roots of young seedlings. Younger axile roots, emerging from higher internodes, cause more differences in the values with regard to lateral root growth. These roots have young populations of lateral roots, which are in an exponential growth phase. This is highlighted by the different dynamics of the establishment of axile roots between the two genotypes. The early increase in the axile roots of RIL 372, with a higher growth rate than the axile roots of RIL 15 may have led to the stronger ER_{Ax} of RIL 372 but also contribute to k_{Lat}.

Regardless of these theoretical complications, we identified contrasting genotypes and verified their differences by manual observations. Similar differences among genotypes were reported elsewhere. Hund et al. (2007) characterized 21 temperate maize inbred lines according to the organization of their embryonic root system (the primary and seminal roots) and distinguished among those with a more homogeneous root system (similar primary and

seminal roots) and those with more heterogeneous root systems (lateral roots of the primary root generally longer than the lateral roots of the seminal roots). Furthermore, quantitative trait loci for the organization of the embryonic root system at the V1 stage were identified and highlight the independent inheritance of the root types and the formation of their lateral roots (Hund et al. 2004). The parents of this mapping population, Lo964 and Lo1016, were also characterized by a heterogeneous and a homogenous embryonic root system, respectively. Accordingly, the embryonic root system of RIL 15 is characterized as heterogeneous, with a strong primary root with comparably long and dense first-order lateral roots; The Root system of RIL 372 is characterized as homogeneous with fewer and shorter branches on the primary root, similar to its seminal roots.

Conclusions

The established phenotyping protocol enabled a non invasive measurement of the dynamics of axile and lateral roots. It was shown that errors in root length at a given point in time can be very large if differences in germination are not taken into account. A solution to this is the application of appropriate elongation models to separate the influence of germination and elongation on the final root length. Based on the elongation rates of the population of lateral and axile roots, different genotypes can be identified, as demonstrated for RIL 15 and RIL 372. Using stored images allows for the dissection of growth rates into their underlying causes. The comparably high throughput makes the phenotyping platform suitable for the study of the quantitative inheritance of root morphology or for other screening purposes. However, further efforts are required to i) develop non-invasive techniques with high throughput at a later autotrophic growth stage and ii) develop adequate software packages and protocols to enhance the detailed digital measurement of the root system without excessive manual input.

References

Bonser AM, Lynch J, Snapp S (1996) Effect of phosphorus deficiency on growth angle of basal roots in Phaseolus vulgaris. New Phytol 132:281–288. doi:10.1111/j.1469-8137.1996.tb01847.x

Bourdu R, Grégory N (1983) Etude comparée du début de la croissance chez divers génotypes de maïs. Agronomie 3:761–770. doi:10.1051/agro:19830807

Chassot A, Richner W (2002) Root characteristics and phosphorus uptake of maize seedlings in a bilayered soil. Agron J 94:118–127

Cooper CS, Mac Donald PW (1970) Energetics of early seeling growth in corn (Zea mays L.). Crop Sci 10:136–139

Delées E, Grégory N, Bourdu R (1984) Transition between seed reserves use and photosynthetic supply during development of maize seedlings. Plant Sci Lett 37:35–39. doi:10.1016/0304-4211(84)90199-8

Doussan C, Pierret A, Garrigues E, Pages L (2006) Water uptake by plant roots: II—Modelling of water transfer in the soil root-system with explicit account of flow within the root system—Comparison with experiments. Plant Soil 283:99–117. doi:10.1007/s11104-004-7904-z

Enns LC, McCully ME, Canny MJ (2006) Branch roots of young maize seedlings, their production, growth, and phloem supply from the primary root. Funct Plant Biol 33:391–399. doi:10.1071/FP06029

Gregory PJ, Hutchison DJ, Read DB, Jenneson PM, Gilboy WB, Morton EJ (2003) Non-invasive imaging of roots with high resolution X-ray micro-tomography. Plant Soil 255:351–359. doi:10.1023/A:1026179919689

Hoecker N, Keller B, Piepho HP, Hochholdinger F (2006) Manifestation of heterosis during early maize (Zea mays L.) root development. Theor Appl Genet 112:421–429. doi:10.1007/s00122-005-0139-4

Hund A, Frachboud Y, Soldati A, Frascaroli E, Salvi S, Stamp P (2004) QTL controlling root and shoot traits of maize seedlings under cold stress. Theor Appl Genet 109:618–629. doi:10.1007/s00122-004-1665-1

Hund A, Richner W, Soldati A, Fracheboud Y, Stamp P (2007) Root morphology and photosynthetic performance of maize inbred lines at low temperature. Eur J Agron 27:52–61. doi:10.1016/j.eja.2007.01.003

Hund A, Fracheboud Y, Soldati A, Stamp P (2008a) Cold tolerance of maize seedlings as determined by root morphology and photosynthetic traits. Eur J Agron 28:178–185. doi:10.1016/j.eja.2007.07.003

Hund A, Ruta N, Liedgens M (2008b) Rooting depth and water use efficiency of tropical maize inbred lines, differing in drought tolerance. Plant Soil (in press). doi:10.1007/s11104-008-9843-6

Janssen GJW, VanNorel A, VerkerkBakker B, Janssen R (1995) Detecting resistance to the root-knot nematodes Meloidogyne hapla and M-chitwoodi in potato and wild Solanum spp. Potato Research 38:353–362

Lambers H, Shane MW, Cramer MD, Pearse SJ, Veneklaas EJ (2006) Root structure and functioning for efficient acquisition of phosphorus: Matching morphological and physiological traits. Ann Bot (Lond) 98:693–713. doi:10.1093/aob/mcl114

Liao H, Rubio G, Yan XL, Cao AQ, Brown KM, Lynch JP (2001) Effect of phosphorus availability on basal root shallowness in common bean. Plant Soil 232:69–79. doi:10.1023/A:1010381919003

Liao H, Yan XL, Rubio G, Beebe SE, Blair MW, Lynch JP (2004) Genetic mapping of basal root gravitropism and phosphorus acquisition efficiency in common bean. Funct Plant Biol 31:959–970. doi:10.1071/FP03255

Liu JC, Li JS, Chen FJ, Zhang FS, Ren TH, Zhuang ZJ, Mi GH (2008) Mapping QTLs for root traits under different nitrate levels at the seedling stage in maize (Zea mays L.). Plant Soil 305:253–265. doi:10.1007/s11104-008-9562-z

Manschadi AM, Christopher J, Devoil P, Hammer GL (2006) The role of root architectural traits in adaptation of wheat to water-limited environments. Funct Plant Biol 33:823–837. doi:10.1071/FP06055

Manschadi AM, Hammer GL, Christopher JT, deVoil P (2008) Genotypic variation in seedling root architectural traits and implications for drought adaptation in wheat (Triticum aestivum L.). Plant Soil 303:115–129. doi:10.1007/s11104-007-9492-1

McCully ME (1999) Roots in soil: unearthing the complexities of roots and their rhizospheres. Annu Rev Plant Physiol Plant Mol Biol 50:695–718. doi:10.1146/annurev.arplant.50.1.695

McMichael BL, Burke JJ (1998) Soil temperature and root growth. HortScience 33:947–951

Messmer R (2006) The genetic dissection of key factors involved in the drought tolerance of tropical maize (Zea mays L.). Diss. ETH No. 16695., Zurich, Switzerland. http://e-collection.ethbib.ethz.ch/show?type=diss&nr=16695

Pinheiro J, Bates D, DebRoy S, Sarkar D (2004) nlme: Linear and nonlinear mixed effects models. R package version 3.

R Development Core Team (2008) R: A language and environment for statistical computing. R Foundation for Statistical Computing, Vienna, Austria

Richner W, Liedgens M, Bürgi H, Soldati A, Stamp P (2000) In root methods. A handbook. In Smit A, Bengough A, Engels C, Van Noordwijk M, Pellerin S (Eds) A handbook. pp 305–342. Springer

Roumet C, Lafont F, Sari M, Warembourg F, Garnier E (2008) Root traits and taxonomic affiliation of nine herbaceous species grown in glasshouse conditions. Plant Soil 312:69–83. doi:10.1007/s11104-008-9635-z

Thain T (2005) "Histotext", a filter plugin for Adobe Photoshop. http://www.telegraphics.com.au/sw/#histotext.

Tuberosa R, Sanguineti MC, Landi P, Giuliani MM, Salvi S, Conti S (2002) Identification of QTLs for root characteristics in maize grown in hydroponics and analysis of their overlap with QTLs for grain yield in the field at two water regimes. Plant Mol Biol 48:697–712. doi:10.1023/A:1014897607670

Varney GT, Canny MJ (1993) Rates of water-uptake into the mature root-system of maize plants. New Phytol 123:775–786. doi:10.1111/j.1469-8137.1993.tb03789.x

Varney GT, Canny MJ, Wang XL, McCully ME (1991) The branch roots of Zea. 1. 1st order branches, their number, sizes and division into classes. Ann Bot (Lond) 67:357–364

Walter A, Spies H, Terjung S, Kusters R, Kirchgessner N, Schurr U (2002) Spatio-temporal dynamics of expansion growth in roots: automatic quantification of diurnal course and temperature response by digital image sequence processing. J Exp Bot 53:689–698. doi:10.1093/jexbot/53.369.689

Weaver JE (1925) Investigations on the root habits of plants. Am J Bot 12:502–509. doi:10.2307/2435298

Zhu JM, Kaeppler SM, Lynch JP (2005) Mapping of QTLs for lateral root branching and length in maize (Zea mays L.) under differential phosphorus supply. Theor Appl Genet 111:688–695. doi:10.1007/s00122-005-2051-3

Zobel R (2003) Sensitivity analysis of computer-based diameter measurement from digital images. Crop Sci 43:583–591

Zobel RW (2008) Hardware and software efficacy in assessment of fine root diameter distributions. Comput Electron Agric 60:178–189. doi:10.1016/j.compag.2007.08.002

Zobel RW, Kinraide TB, Baligar VC (2007) Fine root diameters can change in response to changes in nutrient concentrations. Plant Soil 297:243–254. doi:10.1007/s11104-007-9341-2